

Density matrix renormalization group (DMRG) for cyclic and centrosymmetric linear chains

Manoranjan Kumar,^{1,*} Dayasindhu Dey,¹ Aslam Parvej,¹ S. Ramasesha,^{2,†} and Zoltán G. Soos^{3,‡}

¹*S. N. Bose National Centre for Basic Sciences,
Block - JD, Sector - III, Salt Lake, Kolkata - 700098, India*

²*Solid State and Structural Chemistry Unit, Indian Institute of Science, Bangalore 560012, India*

³*Department of Chemistry, Princeton University, Princeton, New Jersey 08544, USA*

(Dated: March 2, 2022)

The density matrix renormalization group (DMRG) method generates the low-energy states of linear systems of N sites with a few degrees of freedom at each site by starting with a small system and adding sites step by step while keeping constant the dimension of the truncated Hilbert space. DMRG algorithms are adapted to open chains with inversion symmetry at the central site, to cyclic chains and to weakly coupled chains. Physical properties rather than energy accuracy is the motivation. The algorithms are applied to the edge states of linear Heisenberg antiferromagnets with spin $S \geq 1$ and to the quantum phases of a frustrated spin-1/2 chain with exchange between first and second neighbors. The algorithms are found to be accurate for extended Hubbard and related 1D models with charge and spin degrees of freedom.

I. INTRODUCTION

Since White¹ introduced the density matrix renormalization group (DMRG) method and applied it to the spin-1 Heisenberg antiferromagnetic chain, the technique has been recognized to be a powerful quantitative tool for obtaining the low-energy states of spin chains and ladders or of 1D quantum cell models with charge and spin degrees of freedom. The reviews of Schollwöck² and Hallberg³ present the DMRG method in detail. They include discussions of infinite and finite DMRG algorithms, of the underlying ideas, a careful assessment of approximations, optimization schemes, the inclusion of symmetries, and more. The reviews also discuss the scope of DMRG applications to diverse 1D systems and the relation of DMRG to other numerical and theoretical methods.

The vast majority of DMRG calculations are performed on 1D systems with open boundary conditions (OBC) and an even number of sites N , as proposed by White¹ and sketched in Fig. 1. The infinite algorithm increases the targeted superblock size by two sites per step. The system (S) and environment (E) blocks are combined into a superblock whose Hamiltonian matrix retains the same order independent of the superblock's size. Neither the boundary conditions nor even N should matter in the thermodynamic limit, $N \rightarrow \infty$. In practice, however, DMRG calculations are performed on finite systems and the procedure in Fig. 1 is not optimal for systems with inversion symmetry at the central site.

We discuss in this paper other ways for growing 1D systems. The DMRG algorithms in Section II retain the key steps of renormalized operators, truncation and spanning of the Fock space based on the eigenvalues and eigenvectors of the density matrix, and improving the systems block states by refining the density matrices. We mention three algorithms that differ from Fig. 1. First, open 1D chains with odd N have inversion symmetry at the central site and provide complementary information to re-

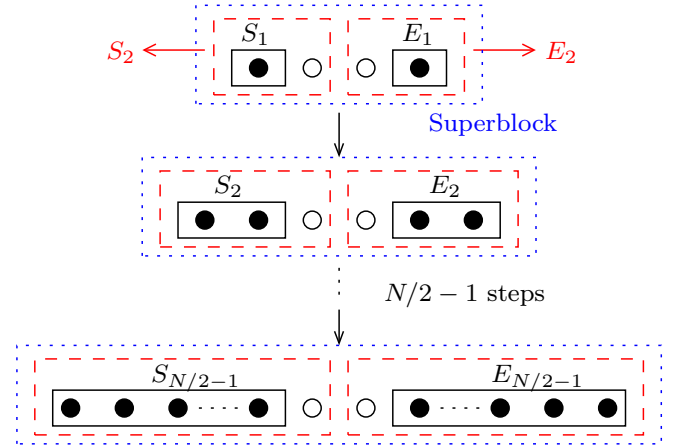


FIG. 1. Schematic representation of the infinite DMRG algorithm: Open circles are new sites added at each step to the system (S) block (left) and environment (E) block (right) until the desired size N is reached.

sults for even N .⁴ Second, periodic boundary conditions (PBC) and translational symmetry are typically assumed in condensed phases, and DMRG can be so modified.⁵ Third, the apparently minor change of adding four instead of two sites in Fig. 1 turns out to be important for weakly coupled quantum systems in certain topologies.⁶

DMRG has principally been applied to (a) spin chains or ladders with short-range exchange interactions and (b) to extended Hubbard models with truncated as well as long-range interactions and to related fermionic models with site energies and/or several sites per unit cell. Here we discuss spin chains using algorithms that also apply to Hubbard models. We consider chains with one spin per unit cell in the thermodynamic limit rather than ladders or chains with several spins per unit cell.

The linear Heisenberg antiferromagnet (HAF) is a

chain of spin- S sites with exchange $J > 0$ between neighbors,

$$H_S(N) = J \sum_{r=1}^{N-1} \vec{S}_r \cdot \vec{S}_{r+1} + J_{1N} \vec{S}_1 \cdot \vec{S}_N. \quad (1)$$

The open chain has no exchange between sites 1 and N ($J_{1N} = 0$), while the ring has $J_{1N} = J$. The $S = 1/2$ chain is a prototypical many-body problem with known exact properties in the thermodynamic limit. Haldane⁷ predicted that integer S chains are gapped, as has been confirmed^{2,3,8} by DMRG and other calculations. HAFs of $S \geq 1$ sites have boundary-induced edge states^{9,10} that are discussed in Section III with the conventional DMRG algorithm for even N and a recent algorithm for odd N .

The $J_1 - J_2$ model with PBC has spin-1/2 sites, J_1 between nearest neighbors and antiferromagnetic $J_2 > 0$ between second neighbors,

$$H(J_1, J_2) = J_1 \sum_r \vec{S}_r \cdot \vec{S}_{r+1} + J_2 \sum_r \vec{S}_r \cdot \vec{S}_{r+2}. \quad (2)$$

The model has been extensively studied: it is frustrated for either sign of J_1 ; it has an exact critical point¹¹ $J_1/J_2 = -4$ between a ferromagnetic and singlet ground state; and a simple exact ground state¹² at $J_1/J_2 = 2$. The quantum phase diagram in Section IV has gapped incommensurate spiral phases with doubly degenerate singlet ground states and spin correlations of finite range as well as gapless phases with nondegenerate ground state and quasi-long-range order.¹³ The ground state degeneracy in finite PBC systems is between states that are even and odd under inversion at sites.

II. TAILORED DMRG ALGORITHMS

The general problem is a 1D chain of N sites with p degrees of freedom per site. Fermionic systems such as Hubbard models have $p = 4$, four states per sites. Spin- S chains have $p = (2S + 1)$ Zeeman levels. The dimension of the Fock space is p^N . The matrix can typically be resolved into sectors with specified symmetries. For example, DMRG algorithms usually conserve only S^z in models that conserve the total spin S . Exact diagonalization (ED) is feasible up to some system size. While it is advantageous to work in small sectors, the dimension increases inexorably with N and precludes the thermodynamic limit that is often sought.

As shown in Fig. 1, two sites are added per step until the desired system size N is reached. Let L be the dimension of the Hilbert space spanned by H in the sector of interest and m be the number of states kept in the system block in the truncated basis. The DMRG approximation gives constant $L' \ll L$ by truncating the Fock space of the system block and renormalizing the operators in the system block at each step. The dimension of the DMRG Fock space is $p^2 m^2$ and the Hilbert space

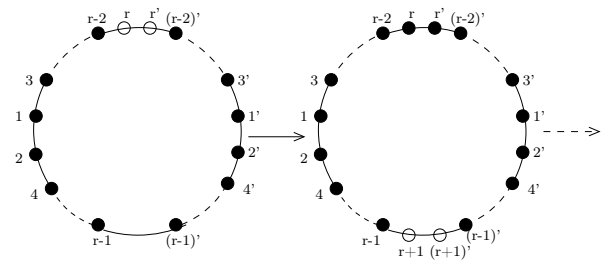


FIG. 2. Schematic representation of an infinite DMRG algorithm for a PBC system: Sites in the left and right blocks are unprimed and primed integers, respectively. Filled circles are old sites; open circles are new sites added at each DMRG step.

in a given S^z sector is usually somewhat smaller. When a superblock of N sites is reached, finite DMRG is performed by systematically and repeatedly repartitioning N sites into a larger “system” block and a smaller “environment” block, and vice versa. This procedure leads to density matrices for different system sizes being obtained from the desired eigenstate of the N -site superblock. The accuracy, quantified by the truncation error,

$$P(m) = 1 - \sum_{j=1}^m \omega_j, \quad (3)$$

increases with m . The sum is over the eigenvalues ω_j of the density matrix. Typical truncation errors are in the range of 10^{-7} to 10^{-9} for $m \sim 100$ to 1000 and can be evaluated for any algorithm.

An infinite DMRG procedure⁵ for systems with PBC and even N is shown in Fig. 2. Two sites are added at each step, alternately in the middle of the top and bottom chains. The motivation is symmetry and ground state properties. Correlation functions may depend on boundary conditions in systems with long-range correlations. Other starting points are possible for rings.¹⁴

More extensive tailoring of the DMRG algorithm is required for Y junctions,¹⁵ systems of $N = 3n + 1$ sites with three arm of n sites that meet at a central site. The infinite algorithm is shown in Fig. 3. The system is one arm plus the central site; the environment is the rest. The junction grows by three sites per step, and the system at one step becomes an arm at the next step. The procedure in Fig. 3 is immediately applicable to OBC chains with odd $N = 2n + 1$, which can be viewed as two arms of n sites and a central site.⁴

Weakly coupled quantum systems are challenging in general and resemble dispersion forces in some ways. The $J_1 - J_2$ model, Eq. 2, discussed in Section IV can be viewed at $J_1 \sim 0$ as two spin-1/2 HAFs on sublattices of even and odd numbered sites. The sublattice spin is $S = 0$ when $N/2$ is even, $S = 1/2$ when $N/2$ is odd. The conventional DMRG algorithm becomes unstable¹⁶ for $J_1/J_2 < 1/2$. Adding four instead of two spins per step restores the stability for sublattices with $S = 0$ at each

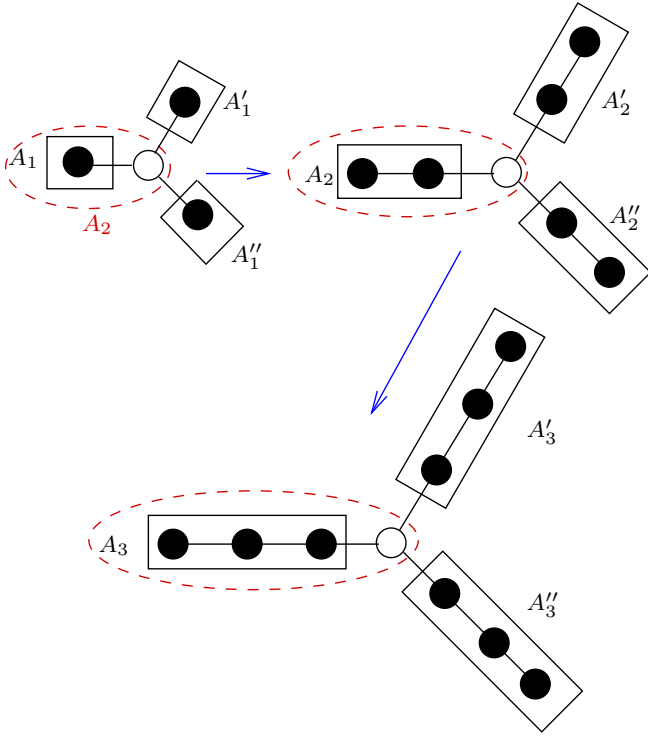


FIG. 3. Schematic representation of the infinite DMRG algorithm for Y junctions with equal arms: At each step, the loop encloses the arm of the next step and the superblock contains a new site, shown as an open dot, and three arms.

step.⁶ The change is crucial when J_1 is small compared to J_2 but not when $J_2 < J_1$.

III. EDGE STATES OF HEISENBERG SPIN CHAINS

We consider H_S in Eq. 1 and set $J = 1$ as the energy unit. The ground state (GS) for OBC has total spin $S_G = 0$ for an even number of sites N and $S_G = S$ for an odd number of sites. There is no energy penalty for parallel spins at sites 1 and N . The chain with PBC has $J_{1N} = J$ and C_N translational symmetry. Antiferromagnetic coupling leads to the smallest possible GS spin: $S_G = 0$ for even N or for integer S , and $S_G = 1/2$ for odd N and half integer S . Exact results in the thermodynamic limit for the $S = 1/2$ HAF refer to even N .

The energy per site is necessarily the same in the thermodynamic limit, but odd N returns $S_G = S$ for OBC and $S_G = 1/2$ for PBC. It follows that HAFs with $S \geq 1$ and OBC have edge states that correspond to boundary-induced spin density waves (BI-SDWs). The energy gap of edge states is⁴

$$\Gamma_S(N) = E_0(S, N) - E_0(0, N), \quad (4)$$

where $E_0(S, N)$ is the lowest energy in the sector with total spin S . Even N leads to $\Gamma_S(N) > 0$. Odd N

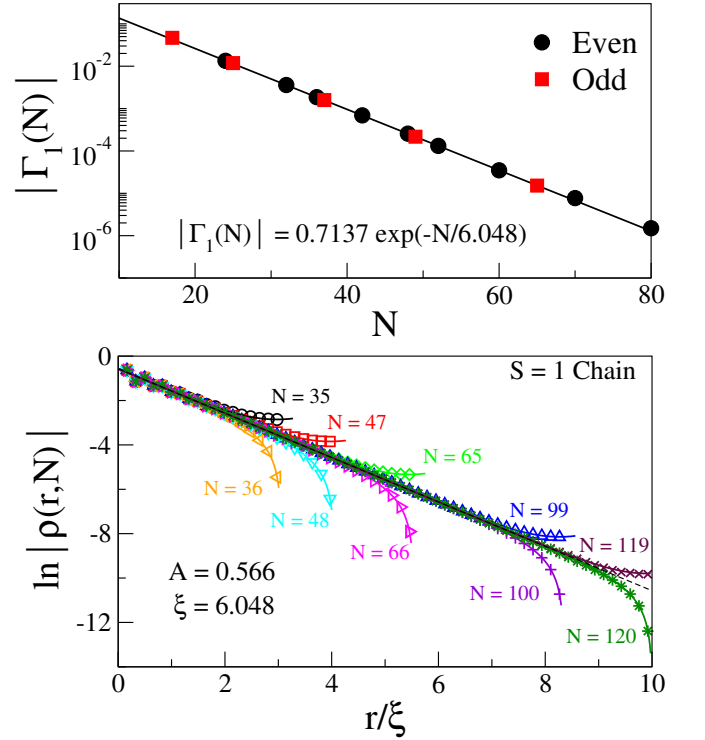


FIG. 4. Upper panel: Singlet-triplet gap $|\Gamma_1(N)|$ of $S = 1$ chains with OBC and N spins in Eq. 1. Lower panel: DMRG results for $|\rho(r, N)|$ to the middle of $S = 1$ chains. Lines are Eq. 7 with $\xi = 6.048$ and $A = 0.566$. Even and odd N deviate from $A \exp(-r/\xi)$ near the middle of chains.

returns $\Gamma_S(N) < 0$ for integer S and $\Gamma_S(N) < 0$ relative to $E_0(1/2, N)$ for half integer S . Since DMRG algorithms conserve S^z rather than S , the most accurate results are for the GS in sectors with increasing S^z and $\Gamma_S(N) > 0$. The singlet (doublet) for $\Gamma_S(N) < 0$ is an excited state in the $S^z = 0$ ($S^z = 1/2$) sector for integer (half integer) S .

According to the nonlinear sigma model, the $S = 1$ chain has an effective spin $s' = 1/2$ at each end.⁹ The size dependence of the singlet-triplet gap is

$$\Gamma_1(N) = (-1)^N J_e \exp(-N/\xi), \quad (5)$$

where ξ is the spin correlation length in the thermodynamic limit and J_e is undetermined. The upper panel of Fig. 4 shows $|\Gamma_1|$ as a function of system size. DMRG returns $\xi = 6.048$ and $J_e = 0.7137$, consistent with previous even- N results.^{8,9} The gap $-\Gamma_1$ for odd N agrees quantitatively with Eq. 5.

The spin density at site r is

$$\rho(r, N) = \langle S_r^z \rangle, \quad r = 1, 2, \dots, N. \quad (6)$$

The expectation value is with respect to the state of interest in the Zeeman sector $S^z = S$. Singlets have $\rho(r, N) = 0$ at all sites. SDWs in $S \geq 1$ chains have

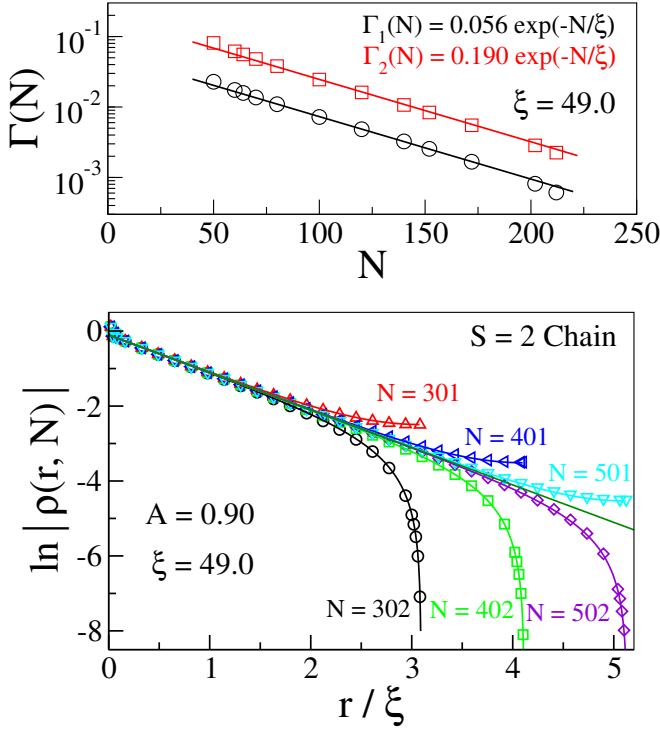


FIG. 5. Upper panel: Edge-states $\Gamma_1(N)$ and $\Gamma_2(N)$ of $S = 2$ chains with OBC and N spins in Eq. 1. Lower panel: DMRG results for $|\rho(r, N)|$ in the $S^z = 2$ sector to the middle of $S = 2$ chains. Lines are Eq. 7 with $\xi = 49.0$ and $A = 0.90$. The chains deviate from $A \exp(-r/\xi)$ in the middle.

equal spin density at r and $N + 1 - r$ by symmetry. We model the spin densities of integer S chains as⁴

$$\rho(r, N) = A(-1)^{r-1} \left(\exp(-r/\xi) - (-1)^N \times \exp(-(N+1-r)/\xi) \right), \quad (7)$$

where A is an amplitude. The SDWs are in phase for odd N , out of phase for even N . The lower panel of Fig. 4 shows $|\rho(r, N)|$ up to the middle of even and odd chains. The lines are Eq. 7 with continuous r and $\xi = 6.048$, $A = 0.566$ for all chains.

The $S = 2$ chain has smaller Haldane gap¹⁷ and hence longer correlations. The gaps in Eq. 4 are Γ_1 to the triplet ($S = 1$) and Γ_2 to the quintet ($S = 2$). The ratio is $\Gamma_2/\Gamma_1 = 3$ for Heisenberg exchange between the effective spins $s' = 1$ at the ends. The panels of Fig. 5 show the gaps for even N and the quintet spin densities to the middle of even and odd chains.⁴ The lines have spin correlation length $\xi = 49.0$ and amplitude $A = 0.90$ in Eq. 7. Even and odd N draw attention to the relative phases of SDWs, and the analysis of spin densities in the middle clarifies the thermodynamic limit. Spin densities are accurately found to $N \sim 500$ while the numerical accuracy⁴ limits the gaps to $N \sim 220$ because Eq. 4 involves small differences between total energies. The calculated ratio $\Gamma_2/\Gamma_1 = 3.4$ is somewhat larger than 3.

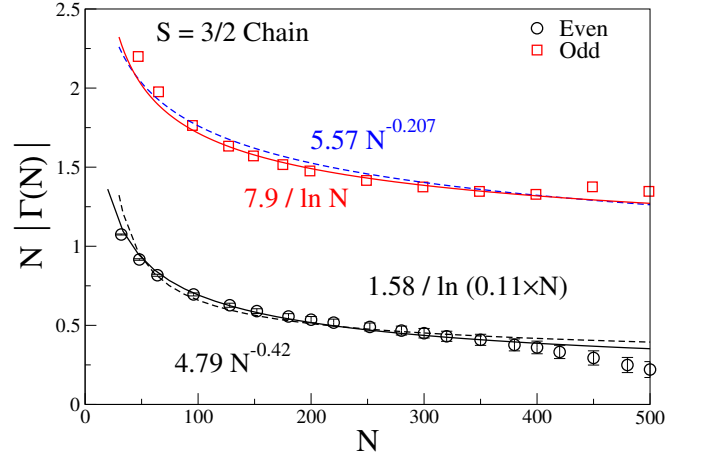


FIG. 6. DMRG results for the gaps $\Gamma_1(N)$ and $|\Gamma_{3/2}(N)|$ for $S = 3/2$ chains with OBC and N spins in Eq. 1. The solid and dashed lines are two parameter fits, with $1.58/\ln 0.11N$ for even N from Ref. 18.

HAF chains with half integer $S \geq 3/2$ are gapless and their edge states are fundamentally different. Even chains have a singlet GS while odd chains have $S_G = S$ and BI-SDWs with half integer $S > 1/2$. The even $S = 3/2$ chain has a gap $\Gamma_1(N)$ that decreases faster than $1/N$ and has been studied¹⁸ to $N = 192$. Odd chains have $-\Gamma_{3/2}(N)$ from the quartet GS to the $S = 1/2$ excited state, which is the first excited state in the $S^z = 1/2$ sector. Both gaps are shown in Fig. 6 up to $N = 450$. The dashed line for even N is the two-parameter fit of Ref. 18, while the solid line is a two-parameter power law. The gap for odd N has larger amplitude and weaker size dependence.

The BI-SDWs of the $S = 3/2$ chain are also qualitatively different. Figure 7 shows the spin densities to the middle of even and odd chains. The total spin density is rigorously 1 for even N and $3/2$ for odd N , as required, but the BI-SDWs are not localized. The sum over all sites of the absolute spin density, $|\rho(N)| = \sum_r |\rho(r, N)|$, diverges in the thermodynamic limit.

In phase BI-SDWs for odd N result in large amplitude at the middle that decreases in Fig. 7 slightly faster than $r^{-1/2}$, while out of phase SDWs cancel for even N . The spin correlation functions^{19,20} of the $S = 1/2$ and $3/2$ HAFs and the size dependence of the amplitude suggests⁴ modeling the spin densities as

$$\rho(r, N) = (-1)^{r-1} C_N \left(\left(\frac{\ln B r}{r} \right)^{1/2} - (-1)^N \times \left(\frac{\ln B(N+1-r)}{N+1-r} \right)^{1/2} \right). \quad (8)$$

The amplitude C_N depends on system size because the SDWs are not localized. The lines for $|\rho(r, N)|$ in Fig. 7 are Eq. 8 with $B = 2$ and the indicated C_N . The spin

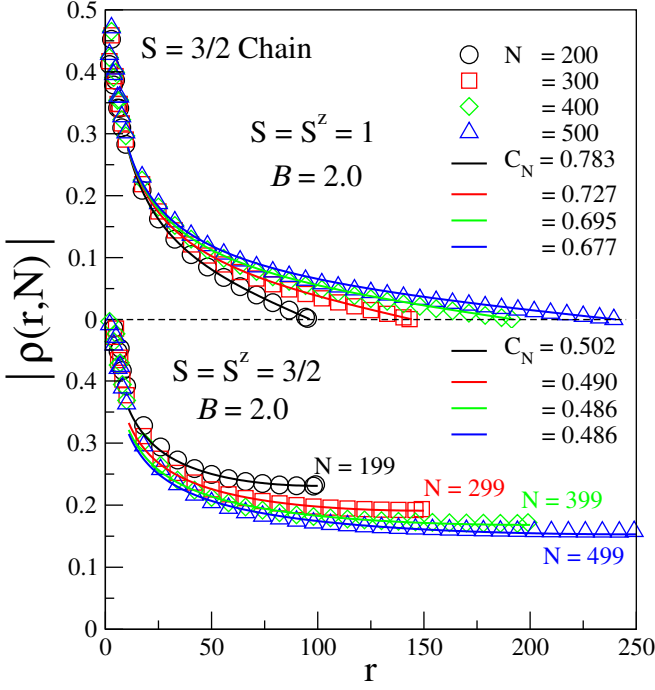


FIG. 7. DMRG results for $|\rho(r, N)|$ to the middle of $S = 3/2$ chains with OBC and N spins in Eq. 1. The lines are Eq. 8 with $B = 2$ and amplitudes C_N .

densities are adequately fit in the central region in either case. Deviations are limited to $r < 10$ when N is even and to $r < 15$ when N is odd, and such deviations are also seen in Figs. 4b and 5b for the first few sites of integer S chains.

IV. $J_1 - J_2$ MODEL: INCOMMENSURATE AND DECOUPLED PHASES

The $J_1 - J_2$ model, Eq. 2, has been studied in several contexts. The quantum phase diagram in Fig. 8 has exact critical and special points. The thermodynamic limit at $J_2 = 0$, $J_1 > 0$ is a spin-1/2 HAF. The gapless phase has a nondegenerate singlet GS and spin correlations with quasi-long-range order (QLRO(π)) at wave vector $q = \pi$. The ferromagnetic phase with $J_1 < 0$ and LRO(0) extends to the exact critical point¹¹ $P1 = J_1/J_2 = -4$. The gapless phase at $J_1 = 0$ has QLRO($\pi/2$) and corresponds to spin-1/2 HAFs on sublattices of even and odd-numbered sites. The exact GS at the Majumdar-Ghosh point,¹² $J_1/J_2 = 2$, are doubly degenerate and very simple: They are the two Kekulé valence bond diagrams of organic chemistry in which adjacent spins are singlet paired, $(\alpha\beta - \beta\alpha)/\sqrt{2}$. The gapped dimer phase has finite-range correlations at $q = \pi$ and spontaneously broken inversion symmetry at sites. The initial studies focused on the critical point²³⁻²⁵ $P4 = J_1/J_2 = 4.148$ where a singlet-triplet gap E_m opens, the GS becomes

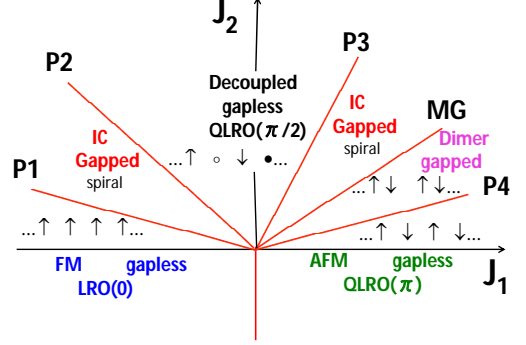


FIG. 8. Quantum phase diagram of $H(J_1, J_2)$, Eq. 2, with critical points P1-P4 at $J_1/J_2 = -4, -1.24, 0.44$ and 4.148 . The exact point P1 is between a gapless ferromagnetic phase and a gapped incommensurate (IC) phase. The gapless decoupled phase is between P2 and P3; open and closed circles denote spins pointing in and out of the plane. The gapped IC phase extends to the MG point, $J_1 = 2J_2$, and the gapped dimer phase to P4, beyond which lies a gapless phase with quasi-long-range order.

doubly degenerate and range of spin correlations becomes finite.

The wave vector q_G of GS spin correlations evolves from $q_G = 0$ at $P1$ to π at MG. The gapped incommensurate spiral phases have doubly degenerate GS with $\pm q_G$. The discussion so far is not at all controversial. There has been disagreement, however, about the critical points P2 and P3 that delimit the decoupled phase in Fig. 8. Field theories^{16,21,22} have restricted the phase to the point $J_1 = 0$ using renormalization group flows to distinguish between gapped and gapless phases. The singlet-triplet gap is very small indeed for $J_1 \sim 0$, far beyond numerical methods, and field theory also entails approximations. Another approach to the phases at small J_1 is to focus on GS degeneracy. The values of P2, P3 in Fig. 8 are mainly based on degeneracy.¹³

Finite $J_1 - J_2$ models of $N = 4n$ spins have discrete wave vectors that change in steps of $\pi/2n$ between $q = 0$ and $\pm\pi$ in the first Brillouin zone. The singlet GS is nondegenerate except at $2n$ values of J_1/J_2 between -4 and 2 where it is doubly degenerate, even and odd, $\sigma = \pm 1$, under inversion at sites.¹³ The first and last degeneracy are at $J_1/J_2 = -4$ and 2 , respectively, for any system size. Increasing J_1/J_2 generates a staircase of $2n$ steps at which q_G changes by $\pi/2n$.

ED is limited to $N = 28$ in our calculations. To study larger $N = 4n$ systems, we evaluate the static structure

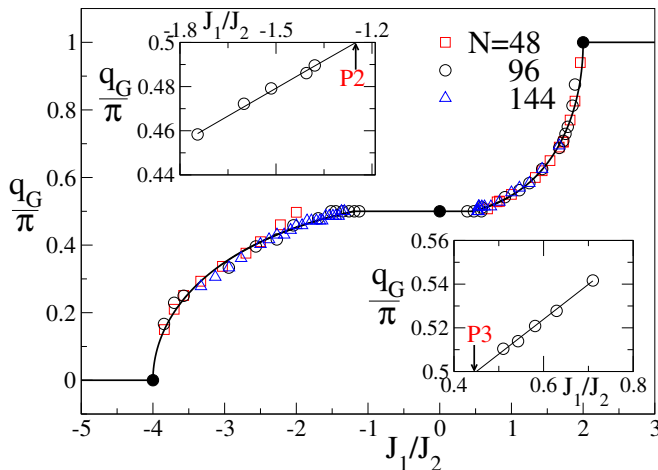


FIG. 9. DMRG results for the wave vector q_S of GS correlations as a function of J_1/J_2 in models with PBC and $N = 4n$ spins in Eq. 2. Closed circles are exact in the thermodynamic limit. The insets show to $N = 192$ the J_1/J_2 values at which the q_S/π plateau is reached in a step $2/N$ at $J_1 < 0$ and left at $J_1 > 0$; linear extrapolation give the critical points $P2$ and $P3$. The line is discussed in Ref. 13.

factor $S(q)$, with q varying from 0 to $\pm\pi$ in steps of $\pi/2n$

$$S(q) = \sum_r \langle \vec{S}_0 \cdot \vec{S}_r \rangle \exp(-irq). \quad (9)$$

The expectation values are in the singlet GS of systems with PBC and $-4 \leq J_1/J_2 \leq 2$. The correlation functions depend only on the separation r between spins. The structure factor peaks¹³ at $q = q_G$ except in the immediate vicinity of $J_1/J_2 = 2$.

DMRG calculations yield $S(q)$ and its maximum q_G as a function of J_1/J_2 . Results to $N = 144$ are shown in Fig. 9. The line is a fit¹³ that takes into account the square-root singularities at -4 and 2 . The $q_G = \pi/2$ plateau is particularly important. The insets show up to $N = 192$ when the plateau is reached at $J_1/J_2 < 0$ and left at $J_1/J_2 > 0$. Linear extrapolation gives the critical points $P2 = -1.24$ and $P3 = 0.44$ in Fig. 8. Finite size and discrete q are advantageous here since q_G is exactly $\pi/2$ and the GS is nondegenerate until q_G changes by $\pm\pi/2n$. The gapless decoupled phase in the interval $-1.24 \leq J_1/J_2 \leq 0.44$ requires a modest extrapolation when viewed in terms of GS degeneracy.

Okamoto and Nomura²³ evaluated $P4$ by noting that a doubly degenerate GS in the dimer phase requires two singlets at lower energy than the lowest triplet. ED to $N = 24$ gave J_1/J_2 at which the singlet excited state and the triplet are degenerate. The weak size dependence

of the crossing allowed accurate extrapolation to $P4 = 4.148$. ED,²³ DMRG²⁴ and field theory²⁵ are in excellent agreement for $P4$.

ED to $N = 28$ for excited state crossings²⁶ also returns estimates for $P2$ and $P3$. The size dependence is stronger but entirely consistent with critical points based on GS degeneracy. As for $P4$, the singlet GS has $q_G = \pi$ for $J_1/J_2 \geq 2$ and $P4$ is related to the divergence of $S(\pi)$ in the QLRO(π) phase. Spin correlations are limited to nearest neighbors at the MG point, where $S_{MG}(\pi) = 3/2$ is exact. The peak $S(\pi)$ increases for $J_1/J_2 > 2$ as the range of spin correlations increases and it diverges at $P4$ in the thermodynamic limit.²⁶ QLRO(q_G) phases have divergent $S(q_G)$.

The spin correlations in Eq. 9 were obtained with a DMRG algorithm for PBC. The largest separation is $r = 2n$ for $N = 4n$. Correlations in OBC systems are typically computed as close to the center as possible in order to minimize end effects; $r = 2n$ requires sites n and $3n$ in systems of $4n$ spins. Significant end effects can be demonstrated in half-filled systems of free electrons. There is presumably no problem when N exceeds the range of correlations. It is difficult to assess the accuracy of structure factors based on OBC spin correlations, and PBC is clearly preferable.

V. CONCLUSIONS

As summarized in Section II, there are different ways to grow 1D systems with infinite DMRG algorithms. The physics of the system rather than energy accuracy is the reason for tailored algorithms. The general DMRG methodology holds directly or with minor modification for these algorithms. Comparable truncation errors, $P(m)$ in Eq. 3, are expected and found. The scheme in Fig. 1 grows two sites per step a 1D chain with an even number of sites. The algorithm developed for Y junctions in Fig. 3 also generates a 1D chain, two sites per step, with an odd number of sites. The scheme in Fig. 2 grows a cyclic 1D chain two sites per step. Adding four instead of two sites per steps makes the conventional algorithm applicable to weakly coupled spin-1/2 chains.

ACKNOWLEDGMENTS

MK thanks the Department of Science and Technology, India for the Ramanujan Fellowship SR/S2/RJN-69/2012 for funding computation facility through SNB/MK/14-15/137. SR thanks the DST, India for support of this work through various grants. ZGS thanks the National Science Foundation, USA.

* manoranj.kumar@bose.res.in

† ramasesh@sscu.iisc.ernet.in

- [†] soos@princeton.edu
- ¹ S R White, *Density Matrix Formulation for Quantum Renormalization Groups*, Phys. Rev. Lett. **69**, 2863 (1992).
 - ² U Schollwöck, *The density-matrix renormalization group*, Rev. Mod. Phys. **77**, 259 (2005).
 - ³ K Hallberg, *New trends in density matrix renormalization*, Adv. Phys. **55**, 477 (2006).
 - ⁴ D Dey, M Kumar and Z G Soos, *Boundary-induced spin density waves in linear Heisenberg antiferromagnetic chains with $S \geq 1$* , arXiv:1606.05054
 - ⁵ M Kumar, S Ramasesha and Z G Soos, *Tuning the bond-order wave phase in the half-filled extended Hubbard model*, Phys. Rev. B **79**, 035102 (2009).
 - ⁶ M Kumar, Z G Soos, D Sen and S Ramasesha, *Modified DMRG algorithm for the zigzag spin-1/2 chain with frustrated antiferromagnetic exchange: Comparison with field theory at large J_2/J_1* , Phys. Rev. B **81**, 104406 (2010).
 - ⁷ F D M Haldane, *Continuum dynamics of the 1-D Heisenberg antiferromagnet: Identification with the $O(3)$ nonlinear sigma model*, Phys. Lett. **93A**, 464 (1983).
 - ⁸ S R White and D A Huse, *Numerical renormalization-group study of low-lying eigenstates of the antiferromagnetic $S = 1$ Heisenberg chain*, Phys. Rev. B **48**, 3844 (1993).
 - ⁹ E H Sørensen and I A Affleck, *Equal-time correlations in Haldane-gap antiferromagnets*, Phys. Rev. B **49**, 15771 (1994).
 - ¹⁰ T K Ng, *Edge states in antiferromagnetic quantum spin chains*, Phys. Rev. **50**, 555 (1994).
 - ¹¹ T Hamada, J Kane, S Nakagawa and Y Natsume, *Exact Solution of the Ground State for the Uniformly Distributed RVB in One-Dimensional Spin-1/2 Heisenberg Systems with Frustration*, J. Phys. Soc. Japan **57**, 1891 (1988).
 - ¹² C K Majumdar and D K Ghosh, *On Next-Nearest-Neighbor Interaction in Linear Chain. II*, J. Math. Phys. **10**, 1399 (1969).
 - ¹³ Z G Soos, A Parvej and M Kumar, *Numerical study of incommensurate and decoupled phase of spin-1/2 chains with isotropic exchange J_1 , J_2 between first and second neighbors*, J. Phys.: Condens. Matter **28**, 175603 (2016).
 - ¹⁴ D Dey, D Maiti and M Kumar, *An Efficient Density Matrix Renormalization Group Algorithm for Chains with Periodic Boundary Condition*, arXiv:1605.09301.
 - ¹⁵ M Kumar, A Parvej, S Thomas, S Ramasesha and Z G Soos, *Efficient density matrix renormalization algorithm to study Y junctions with integer and half integer spin*, Phys. Rev. B **93**, 075107 (2016).
 - ¹⁶ S R White and I Affleck, *Dimerization and incommensurate spiral spin correlations in the zigzag spin chain: Analogies to the Kondo Lattice*, Phys. Rev. B **54**, 9862 (1996).
 - ¹⁷ H Nakano and A Terai, *Reexamination of Finite-Lattice Extrapolation of Haldane Gaps*, J. Phys. Soc. Jpn. **78**, 014003 (2009).
 - ¹⁸ G Fáth, Ö Legaza, P Lajkó and F Iglói, *Logarithmic delocalization of end spins in the $S = 3/2$ antiferromagnetic Heisenberg chain*, Phys. Rev. B **73**, 214447 (2006).
 - ¹⁹ K Hallberg, X Q G Wang, P Horsch and A Moreo, *Critical Behavior of the $S = 3/2$ antiferromagnetic Heisenberg chain*, Phys. Rev. Lett. **76**, 4955 (1996).
 - ²⁰ I Affleck, D Gepner, H J Schultz and T Ziman, *Critical behavior of spin- s Heisenberg antiferromagnetic chains: analytic and numerical results*, J. Phys. A: Math. Gen. **22**, 511 (1989).
 - ²¹ C Itoi and S Qin, *Strongly reduced gap in the zigzag spin chain with a ferromagnetic interchain coupling*, Phys. Rev. B **63**, 224423 (2001).
 - ²² S Furukawa, M Sato, S Onoda and A Furusaki, *Ground-state phase diagram of a spin-1/2 frustrated ferromagnetic XXZ chain: Haldane dimer phase and gapped/gapless chiral phases*, Phys. Rev. B **86**, 094417 (2012).
 - ²³ K Okamoto and K Nomura, *Fluid-dimer critical point in $S = 1/2$ antiferromagnetic Heisenberg chain with next nearest neighbor interactions*, Phys. Lett. A **169**, 433 (1992).
 - ²⁴ R Chitra, S K Pati, H R Krishnamurthy, D Sen and S Ramasesha, *Density matrix renormalization group studies of spin-1/2 Heisenberg system with dimerization and frustration*, Phys. Rev. B **52**, 6581 (1995).
 - ²⁵ S Eggert, *Numerical evidence for multiplicative logarithmic corrections from marginal operators*, Phys. Rev. B **54**, R9612 (1996).
 - ²⁶ M Kumar, A Parvej and Z G Soos, *Level crossing, spin structure factor and quantum phases of the frustrated spin-1/2 chain with first and second neighbor exchange*, J. Phys.: Condens. Matter **27**, 316001 (2015).